Journal of Applied Electrochemistry **34**: 1249–1258, 2004.

Texture and surface morphology in zinc electrodeposits

K. RAEISSI[1,2,*], A. SAATCHI[1], M.A. GOLOZAR[1] and J.A. SZPUNAR[2]
[1]*Department of Materials Engineering, Isfahan University of Technology, Isfahan 84154, Iran*
[2]*Department of Mining, Metals and Materials Engineering, McGill University, M.H. Wong Building, 3610 University, Montreal, QC, Canada H3H 2B2*
*(*author for correspondence, fax: +98-311-3912752, e-mail: kraeissi@hotmail.com)*

Received 22 march 2004; accepted in revised form 13 july 2004

Key words: AC impedance plots, electrodeposition, Surface morphology, texture, zinc coating

Abstract

The texture and morphology of zinc coatings electrodeposited on low carbon steel substrate have been studied. The predominant texture component of zinc coating at low overpotentials was pyramidal (11.5) and (11.6) non-fiber while at high overpotentials (00.2) fiber component dominated. The morphological analysis of the coating surface indicates that the non-fiber texture component results from epitaxial growth of zinc which develops through 2D nucleation and bunching growth of substrate surface microsteps, while the (00.2) fiber component starts from 3D nucleation and oriented growth to promote the plane having the lowest surface energy (i.e., (00.2)) parallel to the steel substrate surface. Zinc hydroxide adsorption prevents 3D nucleation at low overpotentials and this process favors epitaxial growth of the zinc deposit. At high overpotentials, inhibited zinc adsorption, in addition to increased number of active nucleation sites, promotes strong (00.2) fiber component. Such variation in texture indicates that the electrodeposit texture is strongly dependant on overpotential.

1. Introduction

Zinc electrodeposits are used in numerous applications especially in the automotive industry to improve the corrosion resistance of steel used for car bodies. This coating may have very different properties because of differences in microstructures obtained by varying the deposition conditions. The coating properties such as corrosion resistance, paintability and formability are closely related to the morphology and texture of the coating [1–7, Raeissi et al., submitted for publication]. Various morphologies and textures may develop by changing electrochemical deposition parameters such as current density, temperature, pH, substrate surface preparation and bath composition [7–13]. Although there has been work on the effect of electrochemical variables on the texture of zinc electrodeposits [7–13, Raeissi et al., submitted for publication], texture development and the reasons for its variation with changes of electrochemical parameters are not completely clear.

Park and Szpunar [6, 10] used pole figures to evaluate the texture of zinc electrodeposits in an acid sulfate bath. High intensity of basal (00.2) fiber texture and low intensity of non-fiber pyramidal {10.X} was observed at low current densities using an electropolished steel substrate [6]. An increase in percentage of basal plane texture with increasing current density up to 300 mA cm^{-2} at 50 °C was reported. Vasilakopoulos et al. [4] used X-ray diffraction patterns to calculate relative texture coefficients for different planes of zinc deposited onto chemically polished steel substrate. They reported a major basal texture and some pyramidal {10.X} texture component. They also detected some {11.4} orientation in a particular range of deposition conditions [4].

The aim of this work is to do further structural observation on texture development to better understand the relationship between texture and electrochemical parameters used for electrodeposition. The effect of current density, temperature, pH and coating thickness on the texture of zinc deposited onto electropolished low carbon steel is discussed.

2. Experimental procedure

The substrate was prepared from a commercial cold rolled low carbon steel sheet with a thickness of 1 mm. The specimens were disk shaped with a surface area of 0.85 cm^2. The specimens were sealed in a stainless steel foil sack and annealed at 880 °C for 3 h, and were then mechanically ground down to 600-grit abrasive SiC papers and subsequently electropolished in a solution of 95% acetic acid and 5% percholoric acid for about 2.5–3 min. After electropolishing, the specimens were washed with distilled water and soaked in 10% sulfuric acid for 20 s. Then, the specimens were washed again

with distilled water and immediately placed in the electroplating bath.

The bath composition was $ZnSO_4{\cdot}7H_2O$ (620 g l^{-1}) plus Na_2SO_4 (75 g l^{-1}). The pH of the bath was adjusted to 2 with dilute sulfuric acid. Deposition was conducted in a standard corrosion cell with two graphite counter electrodes and a saturated calomel electrode (SCE) as reference electrode. This electrode was placed close to the cathode surface via a luggin capillary filled with bath solution. The temperature of the cell was maintained at 25 ± 2 °C or 50 ± 2 °C using a water bath. An EG&G (model 263A) computer controlled potentiostat/galvanostat was used to maintain the current density at 10, 100, and 200 mA cm^{-2}. The plating time was set to 1100, 110, and 55 s for the above current densities to produce a constant coating thickness of 5 μm. Potential vs time curves were plotted during the deposition process. Cathodic polarization tests were run with a scan rate of 40 mV s^{-1}. An EG&G AC responser (model 1025) was coupled with potentiostat/galvanostat to read AC impedance resistance. AC impedance tests were taken in a conventional cell with platinum counter electrodes and a SCE as the reference electrode with a similar arrangement as the standard corrosion cell.

A Philips XL30 scanning electron microscope was used to observe the morphology of the deposits. A Nanoscope III AFM was used in contact mode with a silicon nitride tip to reveal the surface topography of the investigated coatings. A Siemens D500 diffractometer was used to determine substrate and coating texture. The diffractometer was operated using Cu-K_α at an accelerating voltage of 40 kV and a current of 40 mA. Three pole figures were measured for the planes of (00.2), (10.0) and (10.1) using the reflection technique in 5° polar and angular intervals. The ODF were calculated using TexTools software and then recalculated pole figures were plotted.

3. Results and discussion

Figure 1 shows the pole figures of zinc electrodeposited at 10, 100, and 200 mA cm^{-2} at 25 °C. A sharp non-fiber

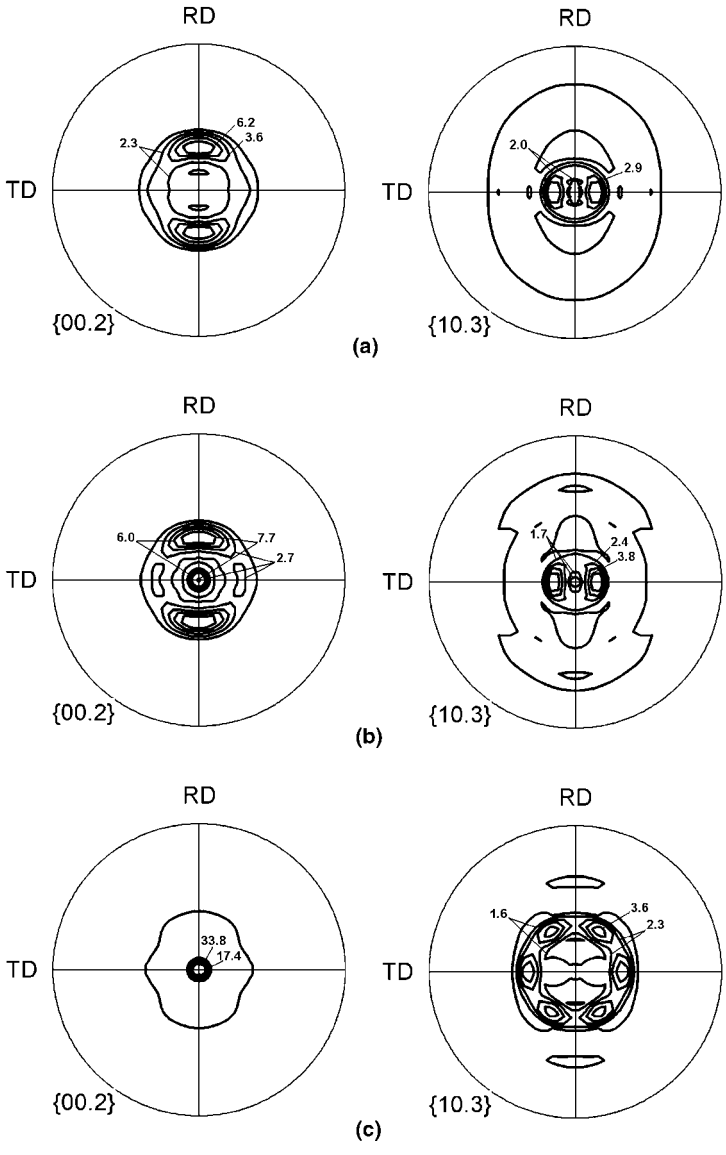

Fig. 1. Pole figures of zinc electrodeposited at 25 °C. (a) 10, (b) 100, and (c) 200 mA cm^{-2}.

texture component, which involves pyramidal (11.5) $< \bar{3}\ \bar{3}.1 >$ and (11.6) $< \bar{3}\ \bar{3}.1 >$ component along with some pyramidal (10.3) $< \bar{3}\ \bar{2}.1 >$ component are evident from the pole figures of the deposit (Figure 1(a) and (b)).

Figure 2 shows the pole figures of steel sheet used as a substrate. The poles of the {110} planes are aligned towards the rolling direction (RD) and tilted about 35° from the center of {110}-pole figure. The non-fiber component of the zinc coating on (00.2) pole figures (Figure 1(a), (b)) is also tilted by the same angle. It may be concluded that the non-fiber texture component is coincident with the orientation of the (110) planes of the steel substrate. It seems that the non-fiber texture component is related to the texture of the substrate. This indicates an epitaxial relationship known as Burger's orientation relationship between the coating and steel substrate. This orientation relationship is described as [14–18]: $(00.2)_\eta // \{110\}_\alpha$ and $< 1\ \bar{2}.0 >_\eta // < 1\ \bar{1}1 >_\alpha$. This orientation relationship is favored when the substrate surface is atomically clean and direct atomic interaction between deposits and substrate can occur [14]. It is expected that the bright surface obtained by electrolytic polishing consists of several sets of {110} terraces [15, 16]. These terraces could provide the Burger's orientation relationship described above [15, 16].

Figure 3 shows the crystallographic relationship between coating and steel substrate through inverse pole figures drawn for Normal directions (ND). The normal directions of steel substrate grains tend towards the [111] crystallographic direction. This means that most of the steel substrate grains have their (111) planes parallel, or nearly parallel, to the sheet surface. On the other hand, the normal directions of zinc crystals tend to be aligned towards the (11.2) direction. This indicates that the (11.5) and (11.6) planes of zinc, which are almost perpendicular to the (11.2) direction, are parallel to the (111) planes of the steel surface. Therefore, epitaxial growth of zinc has developed (11.5) and (11.6) planes parallel to the steel substrate in order to construct the Burger's orientation relationship between the (00.2) planes of zinc and (110) terraces of the steel substrate.

Figure 4 shows the morphology of zinc deposited at 10 mA cm^{-2}. The coating consists of thin-layered hexagonal plates aligned in a specific way on each substrate grain. The zinc deposited on steel is like that on copper,

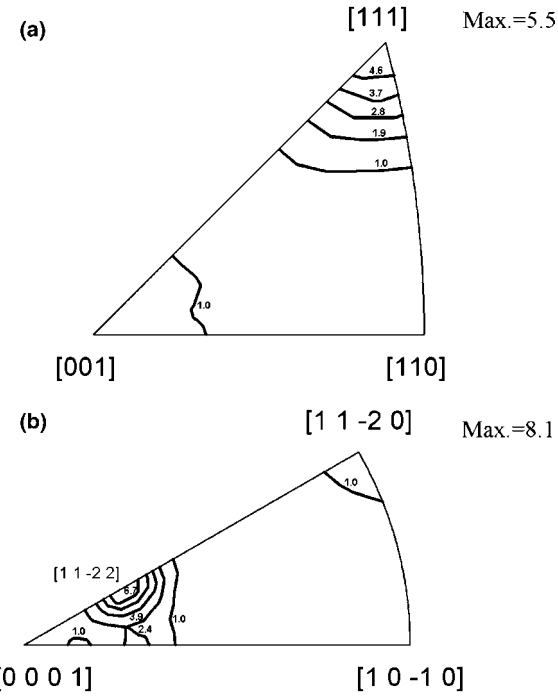

Fig. 3. ND inverse pole figures of (a) steel substrate, (b) zinc electrodeposited at 10 mA cm^{-2} and 25 °C.

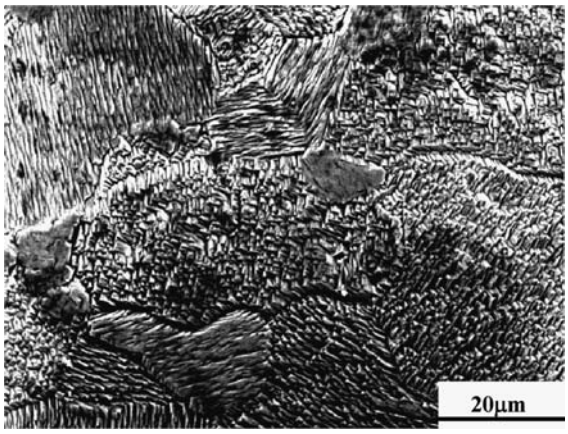

Fig. 4. Morphology of zinc electrodeposited at 25 °C and 10 mA cm^{-2}.

which was described by Itoh [18]. This kind of morphology is called a ridges morphology [6, 10, 19]. The deposit was characterized by the formation of contin-

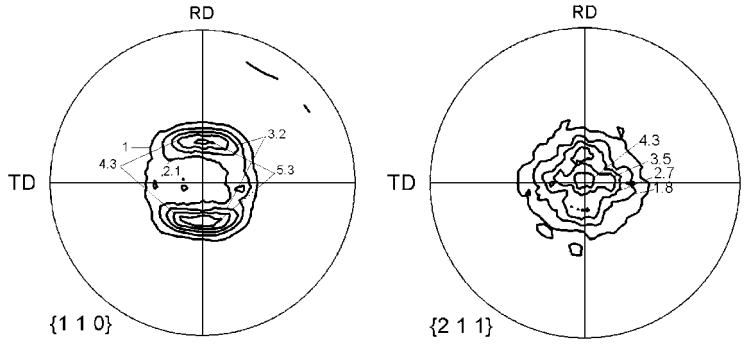

Fig. 2. Pole figures of the low carbon steel substrate.

uous thin sheets of zinc, covering the whole electrode surface without formation of isolated nuclei [18].

Figure 5 shows AFM images of zinc electrodeposited at various times of electrodeposition. These images show the development of the ridge morphology. Numerous tip shape nodules are found after 8 s of electrodeposition at 100 mA cm^{-2}. They are arranged along certain directions that are different for each substrate grain and it seems that these directions depend on the orientation of the substrate grains (Figure 5(b)). Merging of these tips during further development of the coating results in the formation of continuous layers, which are laid on each other (Figure 5(c)). The average roughness (Ra) on each grain increases from 14 to 34 nm for the deposits obtained after 8 and 30 s respectively. The Ra value of the steel substrate was around 7 nm and was similar for grains of different orientation.

It is suggested that zinc atoms are incorporated one after another into microsteps or kinks of vicinal surfaces, without forming the nuclei [18]. This corresponds to 2D nucleation of zinc on the electropolished steel substrate. As discussed earlier, the electropolished surface morphology can be described as microsteps and terraces [15, 16]. Multiplying of these microsteps to form macrosteps is called 'bunching' [19]. The bunching of the microsteps is energetically favored because the edge energy per atom is always higher than the surface energy, and therefore, the process of coalescence of microsteps to form macrosteps will decrease the total surface free energy by decreasing the number of edges [20, 21]. Then, the growth can continue through the build up of these macrosteps. In this way, each grain shows a different variant of alignment of zinc crystallites laid on each other depending on the substrate grain orientation. This kind of nucleation and growth is expected only on electrolytic polished surfaces. Figure 6 shows a schematic drawing to represent the morphology development. After some 2D nucleation of zinc onto surface microsteps in steel, numerous tips are formed and they merge gradually to develop continuous sheets. Since the direction of the steel substrate microsteps are different on each substrate grain, then it is expected that the directional alignment of the sheets will change from one grain to another (Figure 5c). During further growth of the coating a well-defined ridge morphology is developed as illustrated in Figure 4.

The existence of surface microsteps on the substrate surface promotes epitaxial growth of zinc on electropolished surfaces. New steps can be reproduced by 2D nucleation [21]. Therefore, 3D nucleation does not occur on the steel surface and epitaxial growth of zinc occurs via bunching, which produces ridge morphology as described above. This means that the surface

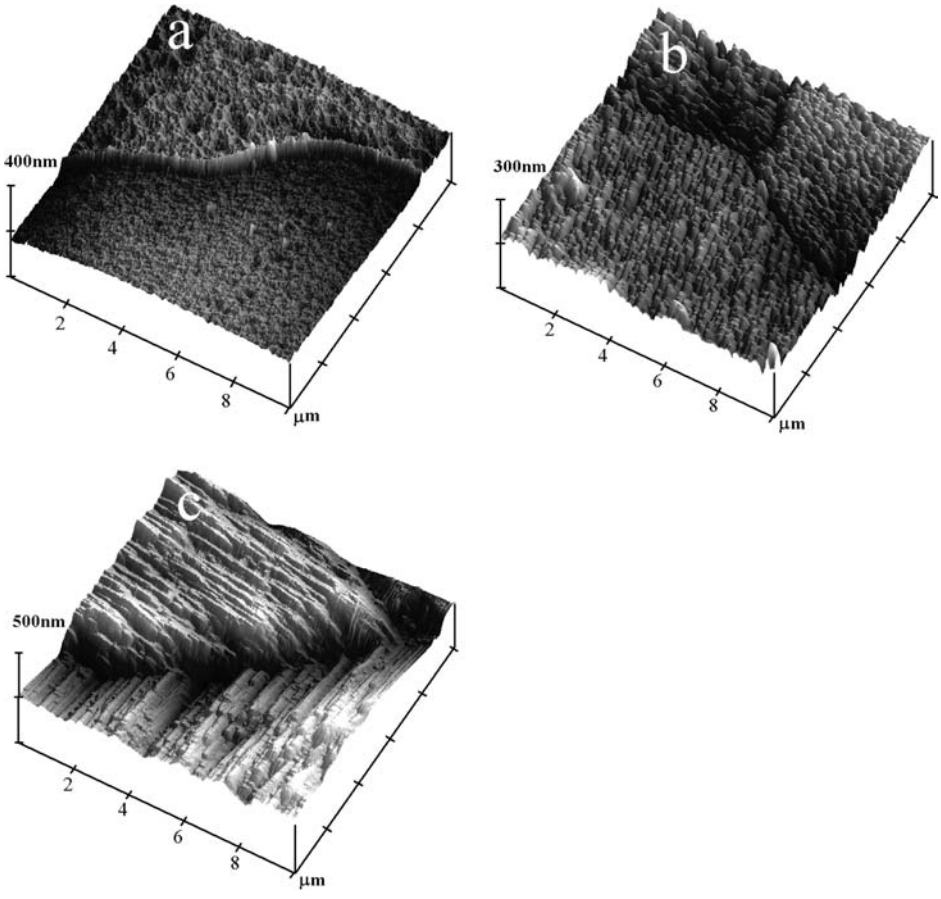

Fig. 5. AFM micrographs of zinc deposited at 100 mA cm^{-2} after, (a) 0, (b) 8, and (c) 30 s.

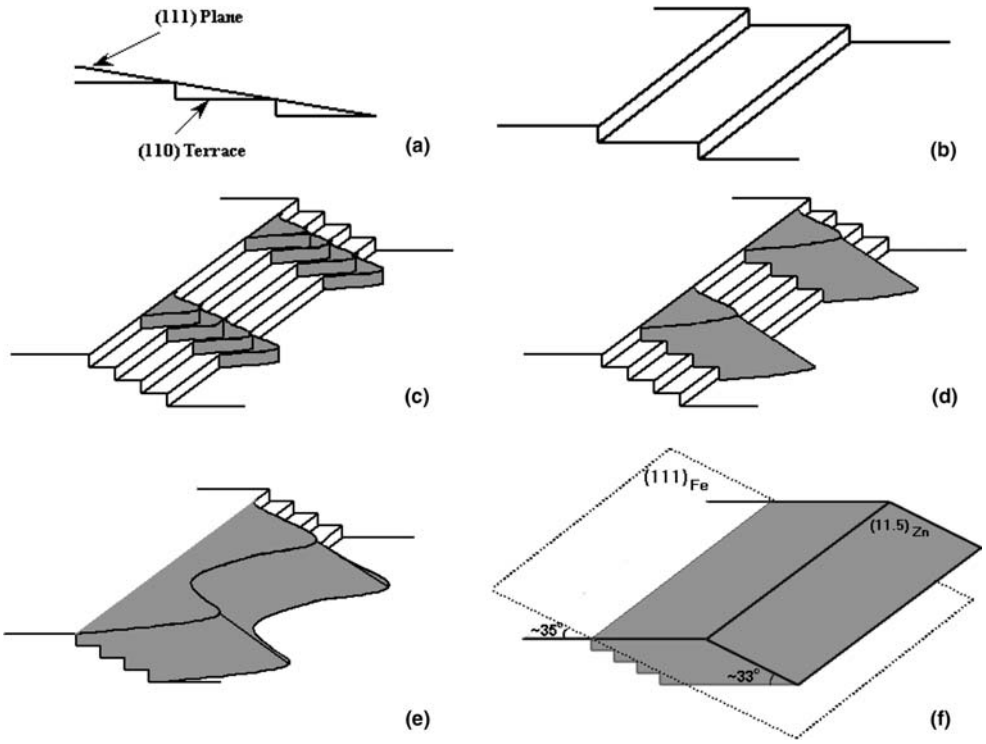

Fig. 6. 2D nucleation of zinc following bunching growth steps to produce non-fiber (11.5) or (11.6) texture components. (a) (111) plan of steel substrate, (b) steel surface shows microsteps and terraces after electropolishing, (c) 2D nucleation of zinc to produce tips onto steel surface microsteps, (d) further growth of tips, (e) the tips merge by further growth, and (f) development of non-fiber texture component on steel surface.

orientation influences epitaxial growth during which the interface stress energy is minimized for individual grains.

Figure 7(a) shows a cross section of zinc deposit obtained at a current density of 100 mA cm^{-2} on steel. Zinc grains are coincident with the steel substrate grains. It can be seen that zinc coating grain boundaries are an extension of the steel substrate grain boundaries. The coincidences points are marked with arrows on Figure 7(a). This observation indicates an epitaxial growth of zinc on steel. During the epitaxial growth of coating on steel substrate, the misfit strain energy for the chosen orientation of both substrate and deposit is minimized [17]. Therefore, it is possible that the non-fiber texture is promoted to minimize the interface energy between the coating and steel substrate [22].

In addition to the sharp non-fiber texture component observed at a deposition current density of 100 mA cm^{-2} (Figure 1(b)), a basal (00.2) fiber texture component is also obtained. This fiber texture component is expected to develop after 3D nucleation and growth [19, 22]. This component is promoted at 100 mA cm^{-2} probably because of high overpotential during zinc deposition. Increase in overpotential strongly affects nucleation rate [21].

Figure 7(b) shows the cross section of zinc and reveals that the epitaxial relationship between the grains of zinc coating and substrate (Figure 7(a)) is not observed. Therefore, non-epitaxial growth of zinc takes place in many grains. This non-epitaxial component is developed via 3D nucleation while epitaxial growth proceeds via 2D nucleation and bunching growth on some grains at 100 mA cm^{-2}.

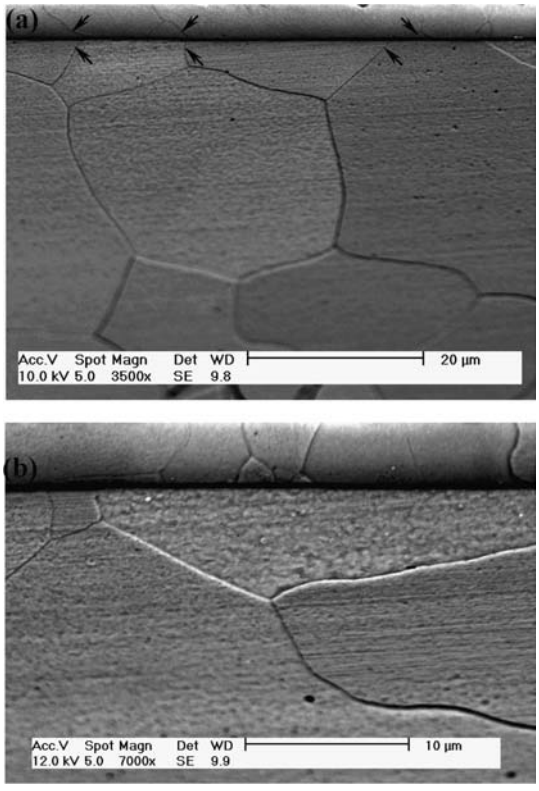

Fig. 7. Cross section of zinc deposited at 10 mA cm^{-2} and 25 °C. (a) epitaxial growth, (b) non-epitaxial growth.

Figures 8 and 9 compare the morphology and topography of these two epitaxial and non-epitaxial components. While the epitaxial growth of zinc with ridges has a Ra value of 28.6 nm (Figure 8(c)), the platelets that resulted from the non-epitaxial growth have Ra values near 10 nm (Figure 9(c)).

Numerous crystals having a platelet morphology grow almost parallel to the substrate to produce a fiber texture component. In this case, the microsteps cannot merge with each other during growth as observed for the ridge morphology. Other authors have also described this kind of morphology [19, 23]. This mode of growth is responsible for the non-epitaxial texture component. The non-epitaxial growth always develops fiber texture components [19].

According to Li and Szpunar [24, 25], development of different fiber textures is possible during the growth of coating due to surface energy differences, which is responsible for the selective growth of grains that have the lowest surface free energy [24, 25]. These authors demonstrated that the growth texture develops to minimize the surface energy of the system, and that the surface energy anisotropy plays an important role in the formation of the fiber textures in iron electrodeposits [24, 25]. As the deposit grows, grains having higher surface energy tend to reduce their surface area while those having low surface energy increase their surface area. As a result, grains with a high surface energy are hindered from growing by the growth of those having a low surface energy [24, 25]. The lowest surface energy in a zinc crystal is for the basal (00.2) plane due to its higher compactness [26]. Therefore, the fiber (00.2) texture component is expected to develop during non-epitaxial growth when no extensive adsorption of hydrogen occurs.

As a rule, the 3D nucleation is linked to overpotential [21]. However, although deposition at 10 mA cm^{-2} occurs with overpotential, 3D nucleation did not occur during deposition. This can be attributed to zinc hydroxide adsorption, which is predominant at low overpotentials.

Figure 10 shows Nyquist plots at 25 °C. These AC impedance readings were obtainded in the 100 kHz–10 m Hz ranges for various DC potentials. These potentials are read directly from the plateau portion of galvanostatic curves for zinc deposition at 10, 100 and 200 mA cm^{-2}. Thus, the AC impedance readings at −1.05, −1.3 and −1.45 V correspond to the deposition potentials at 10, 100, and 200 mA cm^{-2}, respectively. The AC impedance data for −1.05 V show one capacitative loop at high frequencies and two possible inductive loops at low frequencies. The high frequency capacitative loop corresponds to impedance created by

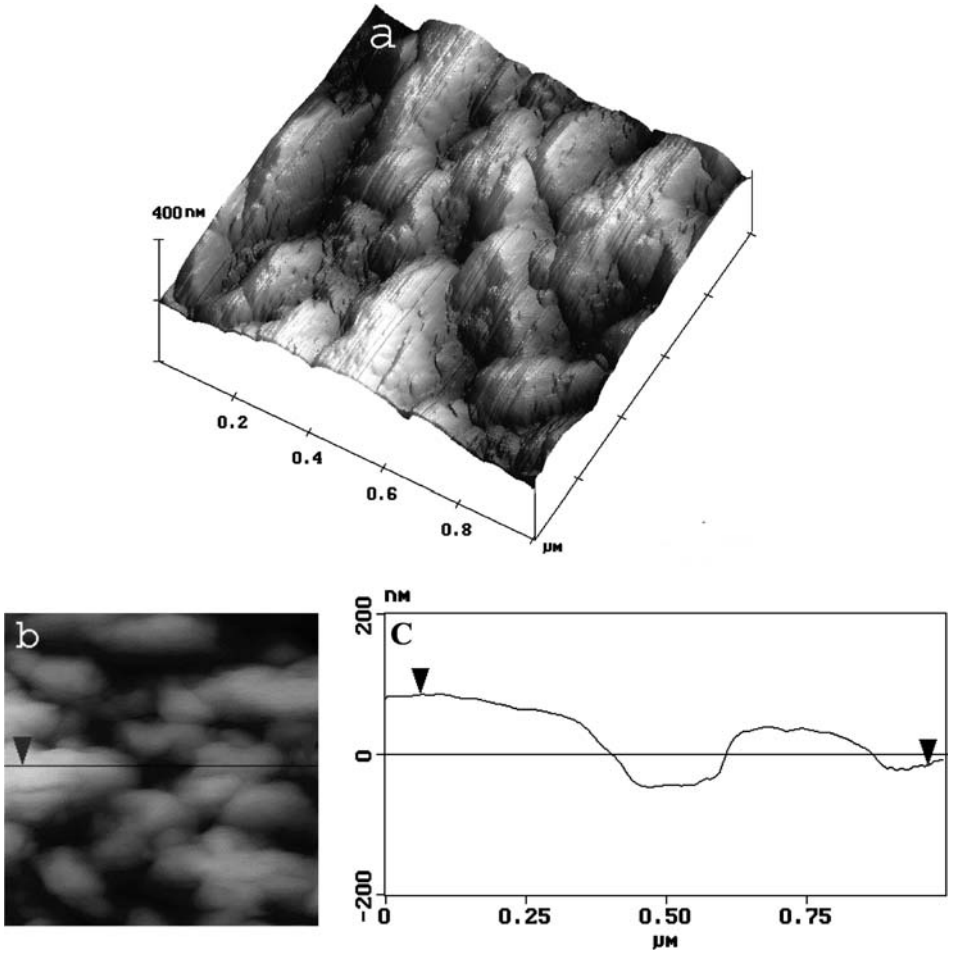

Fig. 8. (a) AFM micrograph of zinc deposited at 100 mA cm^{-2} after 3 s, (b) the top view of the above figure, and (c) the section analysis diagram.

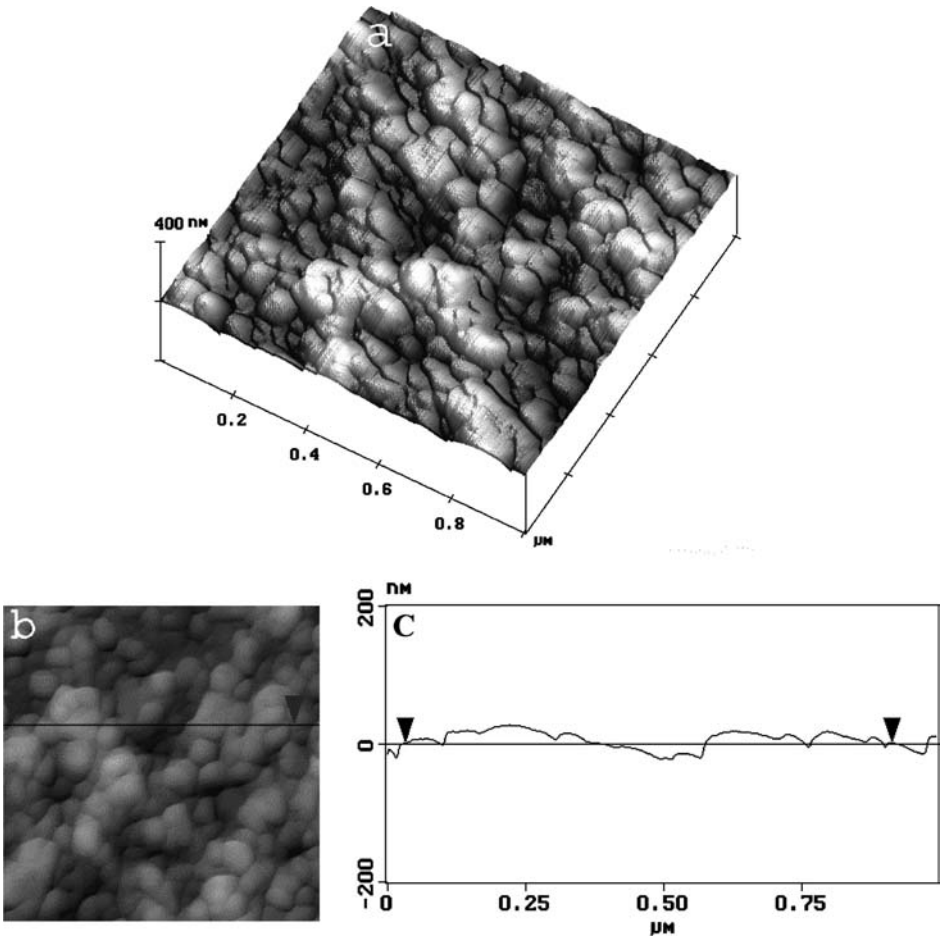

Fig. 9. (a) AFM micrograph from some area of zinc deposited at 100 mA cm^{-2} after 3 s, (b) the top view of the above figure, and (c) the section analysis diagram.

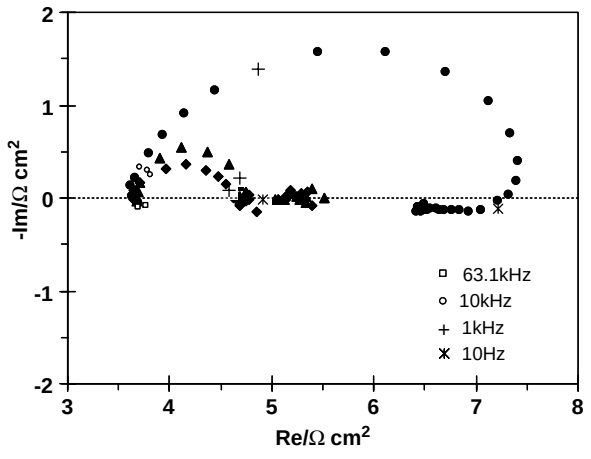

Fig. 10. AC impedance plots at 25 °C. (●)−1.05, (▲) −1.3, and (◆) −1.45 V.

the double-layer capacitance in parallel with the charge transfer resistance [27–29]. The two low-frequency inductive loops correspond to the relaxation of the two coverages Zn_{ad}^{+} and $ZnOH_{ad}$, in the order of decreasing frequencies [27–29]. Near the redox potential (i.e., −1.05 V), the adsorbed zinc hydroxide ($ZnOH_{ad}$) essentially covers the entire electrode surface. In this way, $ZnOH_{ad}$ acts as a blocking adsorbate, which inhibits the 3D nucleation through bouncing the active sites for nucleation [30]. This phenomenon is represented by an inductive loop (loops) at low frequency in the AC impedance diagram at −1.05 V [30]. Thus, inhibited 3D nucleation of zinc by $ZnOH_{ad}$ at 10 mA cm^{-2} could be the reason for epitaxial growth of zinc on the electropolished steel substrate. It would be better to say that at low overpotential, the epitaxial influence of the substrate is so strong that the hydroxide is unable to promote random texture.

Increasing the overpotential (increasing current density) diminished the inductive loop (Figure 10). The chance of 3D nucleation of zinc would increase with overpotential increase not only because of the absence of zinc hydroxide adsorption, but also because of the fact that 3D nucleation is strongly overpotential dependant [21]. Therefore, the substrate lost its epitaxial influence on some of the grains. As a result the (00.2)-fiber texture component is promoted during the growth of these 3D nuclei (Figure 1(b)).

Upon increasing the current density to 200 mA cm^{-2}, the epitaxial texture component was no longer detected (Figure 1(c)). It seems that intensive 3D nucleation at 200 mA cm^{-2} due to overpotential increase prevents

epitaxial growth and hence a strong fiber texture component is developed.

Figure 11 shows the morphology of zinc coating at 200 mA cm^{-2}. Zinc crystallites are predominantly parallel, or nearly parallel, to the steel substrate surface. Figure 11 reveals the morphology of platelets as described above.

Figure 12 shows the pole figures of zinc deposited at 50°C. The intensity of the (00.2) basal texture component is much lower than that deposited at 25 °C. Increasing the temperature to 50 °C decreases the overpotential based on the Butler–Volmer equation [21]. The lower 3D nucleation rate resulting from a decrease in overpotential at 50 °C could be taken into account for explaining the tendency of decreasing strength of the fiber texture. This proves that the basal fiber texture component (i.e. non-epitaxial texture component) is strongly dependant on overpotential.

Figure 12(a) shows very low strength of texture for deposition at 10 mA cm^{-2} and 50 °C. This probably indicates that the zinc hydroxide adsorption onto the steel substrate at potentials very close to the redox potential of zinc has prevented texture formation [30].

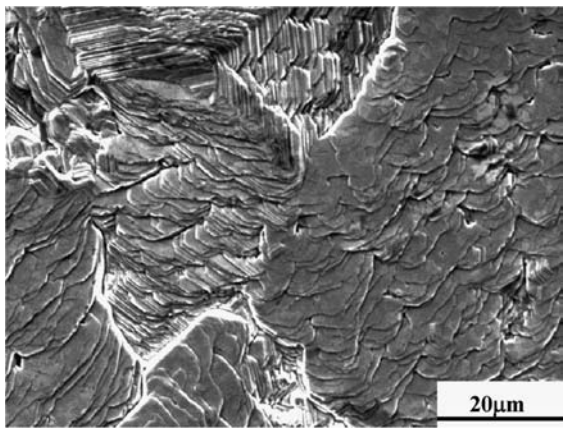

Fig. 11. Morphology of zinc electrodeposited at 25 °C and 200 mA cm^{-2}.

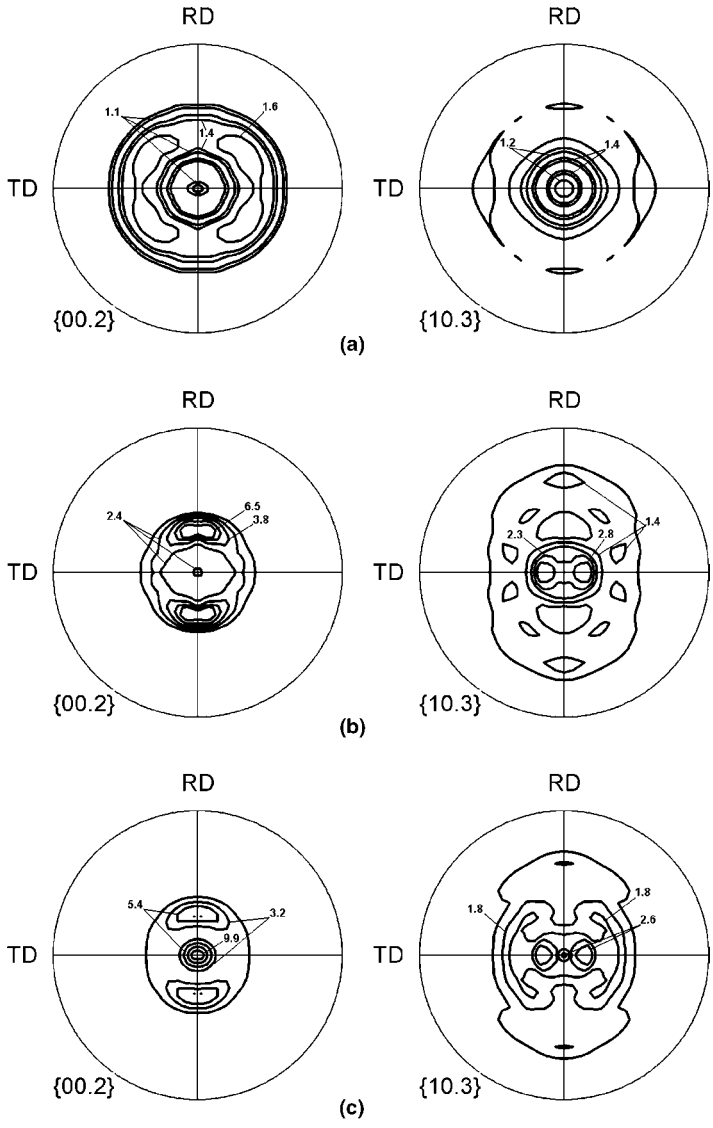

Fig. 12. Pole figures of zinc electrodeposited at 50 °C. (a) 10, (b) 100, and (c) 200 mA cm^{-2}.

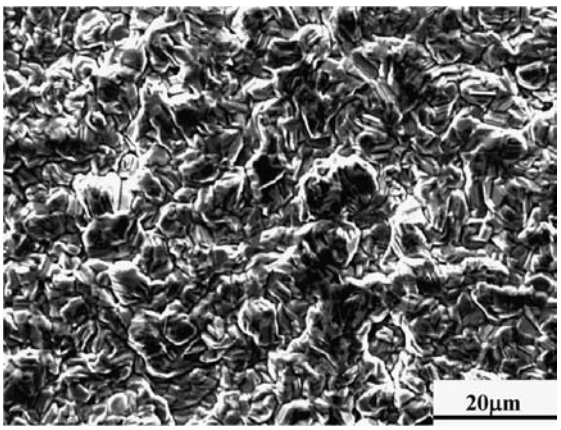

Fig. 13. Morphology of zinc electrodeposited at 50 °C and 10 mA cm^{-2}.

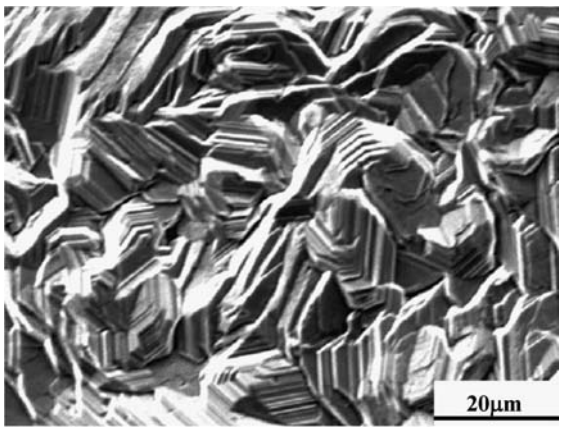

Fig. 15. Morphology of zinc electrodeposited at 25 °C and 100 mA cm^{-2} (40 μm thickness).

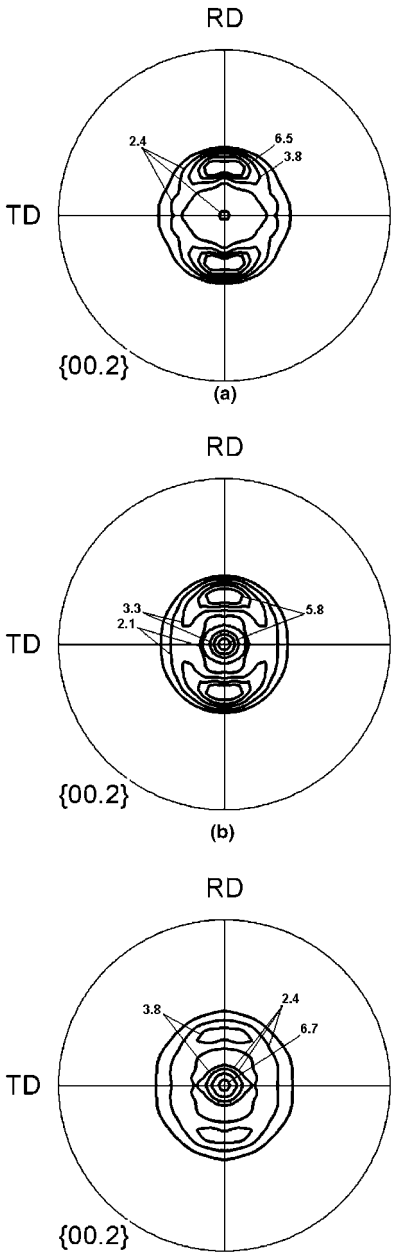

Fig. 14. Pole figures of zinc electrodeposited at 50 °C. (a) 5, (b) 20, and (c) 40 μm.

Figure 13 shows the morphology of this random texture deposit. It shows that the nodular fine-grained deposit is very different from the ridge or platelet morphologies discussed earlier.

According to the above interpretation of non-epitaxial and epitaxial growth, which proceeds with and without 3D nucleation, the basal fiber texture is expected to increase in strength at the expense of the non-fiber texture as the coating becomes thicker. The 3D nucleation and oriented growth takes place after some epitaxial growth because of a high value of misfit strains developed in the deposit [22, 23].

Figure 14 compares the (00.2) pole figures of zinc coatings of 5, 20, and 40 μm. It shows that with increasing thickness, the fraction of fiber (00.2) basal texture component increases. This is due to the non-epitaxial growth of the nuclei generated at some distance from the substrate and minimizing the free energy of the system by faster growth of grains with lower surface free energy.

Figure 15 shows the morphology of the 40 μm thick deposit. The basal zinc crystals have become parallel or nearly parallel to the substrate surface. No evidence of the epitaxial growth (Figure 4) can be found.

It is evident from the above discussion that increasing the overpotential (increasing current density or decreasing temperature) favors 3D nucleation followed by oriented growth and promotes fiber texture components. The (00.2)-plane has lower surface energy in our experimental condition; therefore, it can develop during the growth of 3D nuclei.

4. Conclusion

1. Non-fiber pyramidal (11.5) and (11.6) planes and the fiber (00.2) basal plane are texture components of zinc electrodeposited onto electropolished steel substrates. The formation of these two texture components is explained by epitaxial and non-epitaxial growth.

2. The epitaxial growth of zinc occurs at low overpotentials via 2D nucleation and bunching growth of substrate surface microsteps. The non-epitaxial growth of zinc is predominant at higher overpotential and proceeds through 3D nucleation, which is strongly overpotential dependant. Oriented growth of these 3D nuclei promotes the (00.2) basal texture component. The overpotential obtained for zinc deposition at 200 mA cm^{-2} and 25 °C is high enough to inhibit the growth of the non-fiber texture component and thus a (00.2)-fiber texture is developed.
3. Zinc hydroxide adsorption at low overpotentials inhibits 3D nucleation of zinc. Therefore, only epitaxial growth texture (i.e. non-fiber (11.5) and (11.6) planes) is observed at 10 mA cm^{-2} at 25 °C.

References

1. Y.B. Yim, W.S. Hwang and S.K. Hwang, *J. Electrochem. Soc.* **142** (1995) 2604.
2. S.H. Hong, J.B. Kim and S.K. Lee, *Mat. Sci. Forum* **408–412** (2002) 1025.
3. I. Kim and S. Ch. Hong, Initial and recrystallization textures and microstructures of Zn electrodeposits, *in* Proceeding of the 12th International Conference on Textures of Materials (ICOTOM 12), Montreal, Quebec, Canada, 9–13 August (1999), pp. 956-960.
4. D. Vasilakopoulos, M. Bouroushian and N. Spyrellis, *Trans IMF* **79** (2001), 107.
5. M. Ye, J.L. Delplancke, G. Berton, L. Segers and R. Winand, *Surf. Coat. Technol.* **105** (1998) 148.
6. H. Park and J.A. Szpunar, The influence of deposition parameters on texture in electrogalvanized zinc coatings, *in* Proceeding of the 12th International Conference on Textures of Materials (ICOTOM 12), Montreal, Quebec, Canada, 9–13 August (1999), pp. 1421–1426.
7. K. Deblauwe, A. Deboeck, J. Bollen and W. Timmermans, Influence of processing parameters on the texture of pure zinc electrodeposited coating on steel, *in* Proceeding of the 12th International Conference on Textures of Materials (ICOTOM 12), Montreal, Quebec, Canada, 9–13 August (1999), pp. 1293–1298.
8. N.M. Younan, *J. Appl. Electrochem.* **30** (2000) 55.
9. J.P. Millet, M. Gravria, H. Mazille, D. Marchandise and J.M. Cuntz, *Surf. Coat. Technol.* **123** (2000) 164.
10. H. Park and J.A. Szpunar, *Corr. Sci.* **40** (1998) 525.
11. C.S. Lin, H.B. Lee and S.H. Hsieh, *Metall Trans. A* **31A** (2000) 475.
12. R. Weil, *Annu. Rev. Mater. Sci.* **19** (1989) 165.
13. M. Sagiyama, M. Kawabe and T. Watarabe, *ISIJ Int.* **10** (1990) 99.
14. K. Kamei and Y. Ohmori, *J. Appl. Electrochem.* **17** (1987) 821.
15. Y. Ohmori K. Nakai, H. Ohtsubo, T. Yagi and T. Matsumoto, *ISIJ Int.* **33** (1993) 1196.
16. H. Ohtsubo, T. Matsumoto, K. Nakai and Y. Ohmori, *ISIJ Int.* **34** (1994) 1002.
17. T. Furuhara, N. Sugia and T. Maki *ISIJ Int.* **36** (1996) 584.
18. S. Itoh, N. Yamazoe and T. Seiyama, *Surf. Techol.* 5 (1977) 27.
19. H. Fischer, *Electrodepo. Surf. Treat.* **1** (1972/1973) 319.
20. J. O'M. Bockris, Z. Nagy and D. Drazic, *J. Electrochem. Soc.* 120 (1973) 30.
21. E. Budevski, G. Staikov and W.J. Lorenz, Electrochim. *Acta* **45** (2000) 2559.
22. D.A. Porter and K.E. Easterling, *Phase Transformation in Metals And Alloys* 1992.
23. J. Amblard, M. Froment, G. Maurin, N. Spyrellis and E. Trevisan-Souteyrand, *Electrochim. Acta* **28** (1983) 909.
24. D.Y. Li and Szpunar, *Electrochim. Acta* **42** (1997) 47.
25. D.Y. Li and Szpunar, *Mater. Sci. Forum* **157–162** (1994) 1827.
26. Z.A. Matysina, L.M. Chuprina and S. Yu. Zaginaichenko, *J. Phys. Chem. Solid* **53** (1992) 167.
27. C. Cachet and R. wiart, *J. Electrochem. Soc.* **141** (1994) 131.
28. F. Ganne, C. Cachet, G. Maurin, R. Wiart, E. Chauveau and J. Petitjean, *J. Appl. Electrochem.* **30** (2000) 665.
29. R. Ichino, C. Cachet and R. Wiart, *Electrochim. Acta* **41** (1996) 1031.
30. K. Raeissi, A. Saatchi, and M.A. Golozar, *J. Appl. Electrochem.* **33** (2003) 635.